

# Dynamic Changes in Histone H3 Lysine 9 Methylations

## IDENTIFICATION OF A MITOSIS-SPECIFIC FUNCTION FOR DYNAMIC METHYLATION IN CHROMOSOME CONGRESSION AND SEGREGATION<sup>\*[5]</sup>

Received for publication, May 16, 2005, and in revised form, December 21, 2005. Published, JBC Papers in Press, December 21, 2005, DOI 10.1074/jbc.M505323200

Kirk J. McManus<sup>†1</sup>, Vincent L. Biron<sup>§2</sup>, Ryan Heit<sup>‡</sup>, D. Alan Underhill<sup>§3</sup>, and Michael J. Hendzel<sup>†3,4</sup>

From the <sup>†</sup>Department of Oncology, University of Alberta, Cross Cancer Institute, Edmonton, Alberta T6G 1Z2, Canada and the

<sup>§</sup>Department of Medical Genetics, University of Alberta, Edmonton, Alberta T6G 2H7, Canada

Histone methylation is unique among post-translational histone modifications by virtue of its stability. It is thought to be a relatively stable and heritable epigenetic mark for gene-specific regulation. In this study, we use quantitative *in situ* approaches to investigate the cell cycle dynamics of methylated isoforms of histone H3 lysine 9. Contrary to the expected stability of trimethylated lysines, our results for trimethylated lysine 9 (tMeK9) of H3 demonstrate that the genomic content of this methylation undergoes significant changes as cells progress through mitosis. Unexpectedly, there is a loss of tMeK9 that appears to reflect a robust demethylase activity that is active during the period between anaphase and cytokinesis. Subsequent investigations of mitoses in tMeK9-deficient cells revealed defects in chromosome congression and segregation that are distinct from the increased cohesion at centromeres previously reported in association with the loss of tMeK9. Collectively, these results identify a mitosis-specific trimethylation of Lys<sup>9</sup> in pericentromeric heterochromatin that functions in the faithful segregation of chromosomes.

The core histones (H2A, H2B, H3, and H4) are small basic proteins that form the fundamental building block of chromatin structure, the nucleosome. They function to compact over 2 m of genomic DNA into a nucleus with a diameter of ~10  $\mu$ m. Collectively, the core histones are the targets of more than five different types of post-translational modifications. These include ADP-ribosylation, ubiquitination, phosphorylation, acetylation, and methylation and involve more than 40 different amino acid residues (1). The majority of these modifications occur within the N-terminal tails of the core histones. Most modifications function in the regulation of gene expression by modulating chromatin structure and access of regulatory proteins (reviewed in Refs. 2 and 3). The function of some post-translational histone modifications may be additionally explained by the existence of protein domains found in many key regulatory and transcription factors that specifically recognize and bind acetylated (bromodomain) or methylated (chromodomain) residues (reviewed in Refs. 4–7).

Histone methylation was originally identified in the mid-1960s (8) and was shown to result from histone methyltransferases that catalyze the transfer of methyl groups from *S*-adenosyl-L-methionine onto the  $\epsilon$ -amino group of lysine, arginine, and histidine (9). Histone methyltransferases have been found to be specific for either lysine or arginine residues (10) and the number of methyl groups (*e.g.* mono-, di-, or trimethylations) they attach to the specific amino acid (9) (see also Ref. 11). Interestingly, although all core histones contain arginine and lysine residues, only histones H3 and H4 are good histone methyltransferase substrates *in vivo*. Histone H3 harbors at least six distinct lysine residues that can be methylated (Lys<sup>4</sup>, Lys<sup>9</sup>, Lys<sup>23</sup>, Lys<sup>27</sup>, Lys<sup>36</sup>, and Lys<sup>79</sup>), whereas histone H4 contains at least three target sites (Lys<sup>12</sup>, Lys<sup>20</sup>, and Lys<sup>59</sup>) (1, 2, 12, 13). Recent studies have revealed that histone methylation is an essential process required for the developmental regulation of the metazoan genome (3, 11, 14). For example, methylated Lys<sup>9</sup> (H3) is required for proper heterochromatin protein 1 binding and heterochromatin formation (15–19). In contrast, methylated Lys<sup>4</sup> (H3) preferentially associates with transcriptionally active chromatin (20–22). Unfortunately, however, many of these previous studies fail to distinguish between mono-, di-, or trimethylated species. Nevertheless, in the few studies that have distinguished between various methylation levels, there do appear to be functional distinctions between them. For example, Santos-Rosa *et al.* (23) demonstrated that dimethylated Lys<sup>4</sup> was enriched in active and inactive yeast genes, whereas trimethylated K4 (tMeK4)<sup>5</sup> was only enriched in active genes.

Methylation is known to be much more stable than other posttranslational histone modifications. Metabolic studies using radiolabeled isotopic tracers incorporated into the acetyl-, phospho-, or methyl-groups covalently attached to histones revealed that acetylation and phosphorylation turnover is rapid and can occur within minutes but that methylation appears much more stable. In fact, several research groups found that the methylation turnover rate was not resolved from the turnover of the histones themselves (24–26). However, more recent results have specifically demonstrated that arginine methylation can be subsequently modified by a deimination reaction to yield citrullination (27, 28). Furthermore, it has recently been shown that LSD1, a nuclear homolog of amine oxidases, specifically demethylates dimethylated Lys<sup>4</sup> (29). More recently, it was shown that this demethylase could remove methylation from mono- and dimethylated lysine 9 (29–31). However, to date, lysine 9 trimethylation is considered stable (30).

The trimethylation of lysine 9 has previously been shown to be important in both the regulation of gene expression during interphase

<sup>\*</sup> This work was funded by grants from the Canadian Institutes of Health Research (CIHR) (to M. J. H. and D. A. U.), the Alberta Cancer Board (to M. J. H. and D. A. U.), and the Alberta Heritage Foundation for Medical Research (AHFMR) (to D. A. U.). The costs of publication of this article were defrayed in part by the payment of page charges. This article must therefore be hereby marked "advertisement" in accordance with 18 U.S.C. Section 1734 solely to indicate this fact.

[5] The on-line version of this article (available at <http://www.jbc.org>) contains supplemental Figs. 1–3 and Tables 1–3.

<sup>†</sup> Recipient of graduate studentships from CIHR and AHFMR.

<sup>‡</sup> Supported by a postgraduate scholarship from Natural Sciences and Engineering Research Council.

<sup>§</sup> An AHFMR Scholar.

<sup>4</sup> To whom correspondence should be addressed: Dept. of Oncology, Cross Cancer Institute, 11560 University Ave., Rm. 3332, Edmonton, Alberta T6G 1Z2, Canada. Tel.: 780-432-8493; Fax: 780-432-8892; E-mail: michaelh@cancerboard.ab.ca.

<sup>5</sup> The abbreviations used are: tMeK4, trimethylated lysine 4; dMeK9, dimethylated lysine 9; mMeK9, monomethylated lysine 9; eGFP, enhanced green fluorescent protein; DAPI, 4',6'-diamidino-2-phenylindole; PBS, phosphate-buffered saline; CPTS, copper phthalocyanine 3,4',4'',4'''-tetrasulfonic acid tetrasodium salt; PI, propidium iodide; dn, double null; MEF, mouse embryo fibroblast; IMEF, immortalized mouse embryonic fibroblast; TSI, total signal intensity.

and chromosome segregation (32). Interestingly, the responsible histone lysine methyltransferase, Suv39h1, has been shown to be preferentially recruited to pericentromeric heterochromatin during entry into mitosis (33). In this study, we examined the spatial and temporal dynamics of lysine 9 methylation throughout the cell cycle. Remarkably, we find striking mitosis-specific changes in tMeK9, which rapidly increases as cells enter mitosis, attains maximal levels at metaphase, and rapidly decreases as cells exit mitosis. By early G<sub>1</sub>, the methylation state is returned to its steady-state interphase levels. These changes in lysine 9 trimethylation were even more dramatic in midgestation mouse embryos and nonimmortalized mouse primary cultures. Our results provide the first evidence of changes in histone methylation that preclude the faithful transmission of the methylated lysine residues present in metaphase chromosomes. Furthermore, analysis of mitotic events in cells lacking tMeK9 revealed overall increases in chromosome congression and segregation defects. These defects are distinct from the preponderance of "butterfly chromosomes" reported previously (32) and were also observed in cells treated for 2 h with the methylation inhibitor adenosine dialdehyde.

## MATERIALS AND METHODS

**Cell Culture**—HeLa (human epithelioid cervical carcinoma), IM (male Indian muntjac skin fibroblast), and 10T1/2 (mouse fibroblast) cells were cultured in Dulbecco's modified Eagle's medium plus 10% fetal bovine serum, Ham's F-10 medium plus 20% fetal bovine serum, and  $\alpha$ -minimal essential medium plus 10% fetal bovine serum, respectively, in a 37 °C incubator with 5% CO<sub>2</sub>. Immortalized embryonic fibroblast cell lines from Suv39h1 and Suv39h2 double null embryos were provided by Dr. Thomas Jenuwein and isolated according to established procedures (34).

**Immunofluorescent Labeling**—Asynchronous cells were plated onto sterilized glass coverslips 1 day prior to immunostaining such that they were 50–80% confluent the following day. Cells were fixed, permeabilized, immunofluorescently labeled, and mounted as detailed elsewhere (35).

The following primary antibodies were used at the dilutions indicated: anti-mMeK9 (1:200; Abcam), anti-dMeK9 (1:200; Abcam), anti-tMeK9 (1:200; Abcam), anti-trimethylated Lys<sup>27</sup> (1:500; Abcam), anti-centromeric antigen (1:1000; Dr. G. Chan), and anti-phosphohistone H3 (Ser<sup>10</sup>) (1:400; Upstate Biotechnology, Inc., Lake Placid, NY). Appropriate secondary antibodies (e.g. mouse or rabbit) conjugated to fluorophores (e.g. Alexa Fluor 488 or Cy-3) were used for visualization of primary antibodies and were purchased from Molecular Probes, Inc. (Eugene, OR) or Jackson ImmunoResearch Laboratories, Inc. and used at dilutions of 1:200.

**Generation of 10T1/2 Cells Stably Expressing H3.3-eGFP**—10T1/2 cells stably transfected with eGFP histone H3.3 were kindly provided by Dr. John Th'ng (Northwestern Ontario Regional Cancer Center, Thunder Bay, Ontario, Canada).

**Adenosine Dialdehyde Treatment**—Live cells were treated with 25 mM adenosine dialdehyde (Sigma), a known methyltransferase inhibitor, for either 1 or 2 h. Cells were fixed, permeabilized, and counterstained with DAPI, and phenotypic abnormalities were manually scored.

**Immunoblot Analysis**—To confirm the availability and accessibility of all methylation epitopes and show their temporal regulation throughout the cell cycle, immunoblot analysis was conducted on protein extracts isolated from asynchronously growing cells and compared with extracts isolated from mitotically arrested cells. HeLa cells were mitotically arrested using 15 nM nocodazole (Sigma) for 12 h. Alternatively,

cells were arrested at the G<sub>1</sub>/S-phase boundary by standard double thymidine block, washed extensively with PBS, and permitted to progress for 4 h prior to a 4-h incubation with either nocodazole (15 nM) or ALLN (40  $\mu$ g/ml; Calbiochem). Approximately  $10 \times 10^6$  cells were harvested as described under "Flow Cytometry," with all centrifugation steps performed at 4 °C. Following the final PBS wash, cells were lysed in Nuclei Buffer containing 250 mM sucrose, 200 mM NaCl, 10 mM Tris-HCl (pH 8.0), 2 mM MgCl<sub>2</sub>, 1 mM CaCl<sub>2</sub>, 1% Triton X-100, and 1 mM phenylmethanesulfonyl fluoride. Nuclei were pelleted and resuspended in 0.4N H<sub>2</sub>SO<sub>4</sub> and placed on ice for 30 min. Nuclear debris was cleared by centrifugation at 14,000 rpm for 10 min. Supernatants were collected and added to 60  $\mu$ l of 1 M Tris (pH 8.0) and 40  $\mu$ l of 10 N NaOH.

The acid-extracted proteins from  $2.0 \times 10^5$  asynchronously growing and mitotically arrested cells were resolved on a 15% SDS-polyacrylamide gel. Equivalent protein loading was confirmed by either Coomassie Blue staining of a parallel gel or by copper phthalocyanine 3,4',4'',4'''-tetrasulfonic acid tetrasodium salt (CPTS) staining as described by Bickar and Reid (36). Proteins were transferred to polyvinylidene difluoride membranes, blocked with 5% nonfat milk, and incubated with the appropriate antibody overnight at 4 °C. Immunoblots were washed three times with TBS containing 1% Tween 20 prior to a 1-h incubation with anti-rabbit horseradish peroxidase (1:10,000; Jackson ImmunoResearch Laboratories). Chemiluminescence was performed as described by the manufacturer (ECL+; Amersham Biosciences).

**Flow Cytometry**—Asynchronous and subconfluent cells were harvested using 0.53 mM EDTA. Cells were pelleted by centrifugation at 1,500 rpm for 5 min and resuspended in PBS. Cells were pelleted and resuspended two additional times prior to aliquoting  $2 \times 10^6$  cells per tube. Cells were pelleted and fixed in 1 ml of 70% ice-cold ethanol. Fixed cells were maintained at 4 °C for up to 1 week prior to analysis. Cell aliquots were immunostained separately with 100  $\mu$ l of a 1:200 dilution of one of the anti-methylation antibodies (listed above) for 30 min. Cells were then washed twice with PBS and incubated with anti-rabbit Alexa Fluor 488 (1:200; Molecular Probes) for 30 min. Cells were washed as above, and cell cycle stages were revealed by staining DNA with 60  $\mu$ M propidium iodide (PI) for 30 min at 37 °C. Cells were pelleted, washed once with PBS, and resuspended in 500  $\mu$ l of PBS prior to flow cytometric analysis using a FACSort (BD Biosciences). Appropriate controls were utilized and included unstained cells, PI-stained only, anti-rabbit Alexa Fluor 488 only, and anti-rabbit Alexa Fluor 488 with PI. Figures were compiled in Adobe Photoshop version 6.0, whereas statistical data were exported and analyzed as detailed below.

**Embryo Immunofluorescence**—Embryonic day 9.5 embryos were collected from CD1 mice (Charles River Laboratories), washed in PBS, and fixed in 4% paraformaldehyde at 4 °C for 18 h. Embryos were cryoprotected in 30% sucrose-PBS, mounted in O.C.T. (Tissue-Tek), and sectioned at 14  $\mu$ m using a Leica CM 1900 cryostat. Sections were immediately fixed in 4% paraformaldehyde for 7 min, washed twice for 10 min in PBS, permeabilized for 30 min in PBS plus 0.1% Triton X-100, blocked in PBS plus 0.1% Triton X-100 with 5% heat inactivated sheep serum for 30 min, and incubated overnight at 4 °C with an appropriate primary antibody. Sections were washed three times for 10 min each in PBS plus 0.1% Triton X-100, blocked for 30 min in PBS plus 0.1% Triton X-100 with 5% heat-inactivated sheep serum, incubated with secondary antibody (Alexa594-goat anti-rabbit; 1:300; Molecular Probes) for 2 h at room temperature, washed three times for 5 min each in PBS plus 0.1% Triton X-100, and mounted with 90% glycerol/PBS/DAPI (1  $\mu$ g/ml). Images were collected as detailed above.

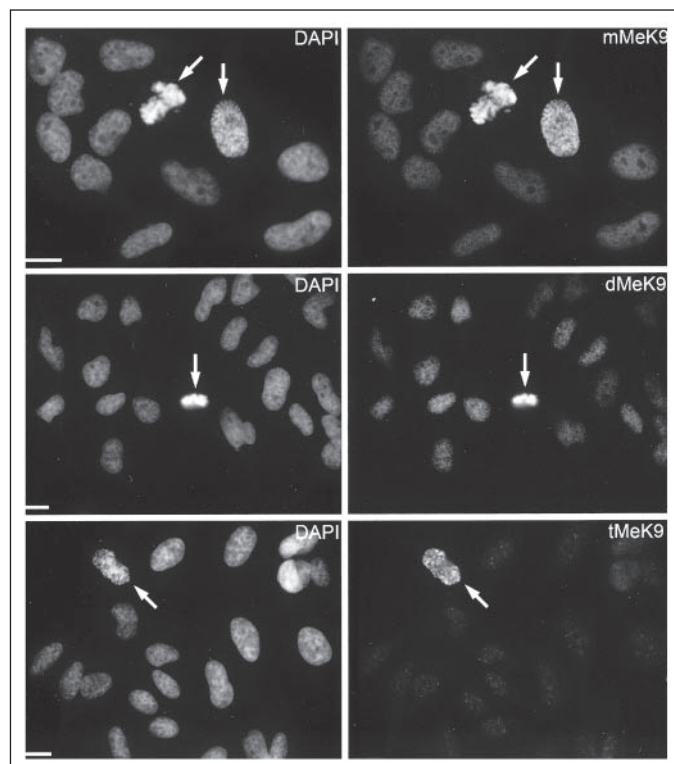


**FIGURE 1. Spatial localization and progression of various methylated lysine 9 (H3) residues.** Representative low resolution ( $\times 40$ ) digital images of HeLa cells immunofluorescently labeled with antibodies directed against mMeK9, dMeK9, and tMeK9. The white arrows identify mitotic cells. Note the increased signal intensities of the mitotic cells over the surrounding interphase cells. The exposure time for the tMeK9 channel was optimized to best present the mitotic signal, and therefore the weaker interphase signals are extremely faint. Scale bar, 7  $\mu\text{m}$ .

**Suv39h1/2 Double Null Immortalized Mouse Embryonic Fibroblasts**—Suv39h1/2 double null (dn) immortalized mouse embryonic fibroblasts (IMEFs) (D5) and IMEF controls (W8) were generously provided by Dr. T. Jenuwein (Research Institute of Molecular Pathology, Vienna, Austria). Cells were cultured in Dulbecco's modified Eagle's medium containing 10% fetal bovine serum and supplemented with 1% nonessential amino acids (Invitrogen) and 0.1 mM  $\beta$ -mercaptoethanol (Sigma). Aberrant mitoses were investigated using an Axioskop 2 plus digital microscope (Carl Zeiss, Inc.) equipped with a plan-neofluar, oil immersion  $\times 40$  (numerical aperture = 0.75) lens. Asynchronous D5 and W8 cells were seeded onto coverslips, paraformaldehyde-fixed, and counterstained with DAPI prior to examination. Based on standard chromosome morphological criteria, mitotic cells were classified as being in metaphase, anaphase, telophase, or cytokinesis/early  $G_1$ . Cells were manually scored as normal or aberrant phenotypes, and the data were tabulated. Aneuploidy was investigated by flow cytometry and was performed as above.

## RESULTS

**Histone Methylation in Asynchronous Cell Cultures**—To explore the possibility of cell cycle-dependent changes in histone H3 lysine 9 methylation states, we examined asynchronous HeLa, IM, and mouse 10T1/2 cells by indirect immunofluorescence using a panel of Lys<sup>9</sup> methylation level-specific antibodies (*i.e.* mono-, di- and trimethylated Lys<sup>9</sup>). The antibodies were deemed to be highly specific for the specified epitope based on indirect immunofluorescence peptide competition assays (supplemental Figs. 1 and 2A). Asynchronous cells provide representa-

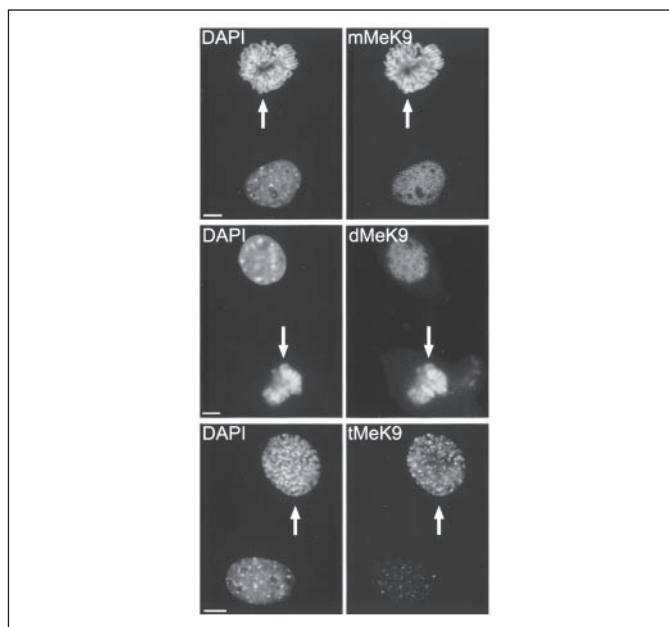


**FIGURE 2. High resolution images of various lysine methylation epitopes in mouse cells.** Representative digital images of 10T1/2 cells immunofluorescently labeled with antibodies directed against mMeK9, dMeK9, and tMeK9. For reference purposes, at least one mitotic cell (indicated by an arrow) has been included for signal intensity comparisons with the interphase cells. The DAPI channel has been included, and pericentromeric heterochromatin is visible as DAPI intense staining regions. Scale bar, 3  $\mu\text{m}$ .

tives of all cell cycle stages on a single slide. A subjective observation of fluorescence intensities can easily be coupled to morphological markers of cell cycle position. This provides a rapid method to survey methylations for potential cell cycle-dependent changes in abundance and has been previously used to identify  $G_2$ - and M-phase-specific changes in histone H3 phosphorylation at serine 10 (37). Fig. 1 illustrates the variation in the intensity of immunofluorescent staining of cells stained with antibodies directed against mono-, di-, and trimethyl modifications at Lys<sup>9</sup> (mMeK9, dMeK9, and tMeK9) of histone H3. There appear to be significant changes in methylation when comparing mitotic and interphase HeLa and 10T1/2 cells labeled with anti-mMeK9, -dMeK9, and -tMeK9 (Figs. 1 and 2). Whereas an apparent increase in methylation will occur solely because of the change in DNA density, the relative change in trimethylation is so dramatic that it is difficult to represent the interphase cell staining without saturating the images of the mitotic cells.

**Phosphorylation of Serine 10 Does Not Increase tMeK9 Detection by Indirect Immunofluorescence**—Surprisingly, the temporal progression pattern of tMeK9 closely resembles that of PhosS10, its neighboring residue. Because there is a possibility that the reactivity of the anti-tMeK9 antibody may be influenced by the presence or absence of PhosS10, we sought to establish whether the anti-tMeK9 antibody would still recognize its cognate epitope in the absence of PhosS10. Accordingly, we developed a calf intestinal alkaline phosphatase assay that is performed *in situ*. Live 10T1/2 cells were permeabilized and treated with or without calf intestinal alkaline phosphatase, paraformaldehyde-fixed, and immunofluorescently labeled with anti-tMeK9. This procedure displaced metaphase cells from the coverslip; however, prophase cells remained adhered to the coverslips and exhibited robust anti-tMeK9 immunostaining in both the presence and absence of PhosS10 (supplemental Fig. 2B). Furthermore, these prophase anti-tMeK9 signal intensities were visually more intense than those of interphase cells on the same coverslips (data not shown). These data estab-



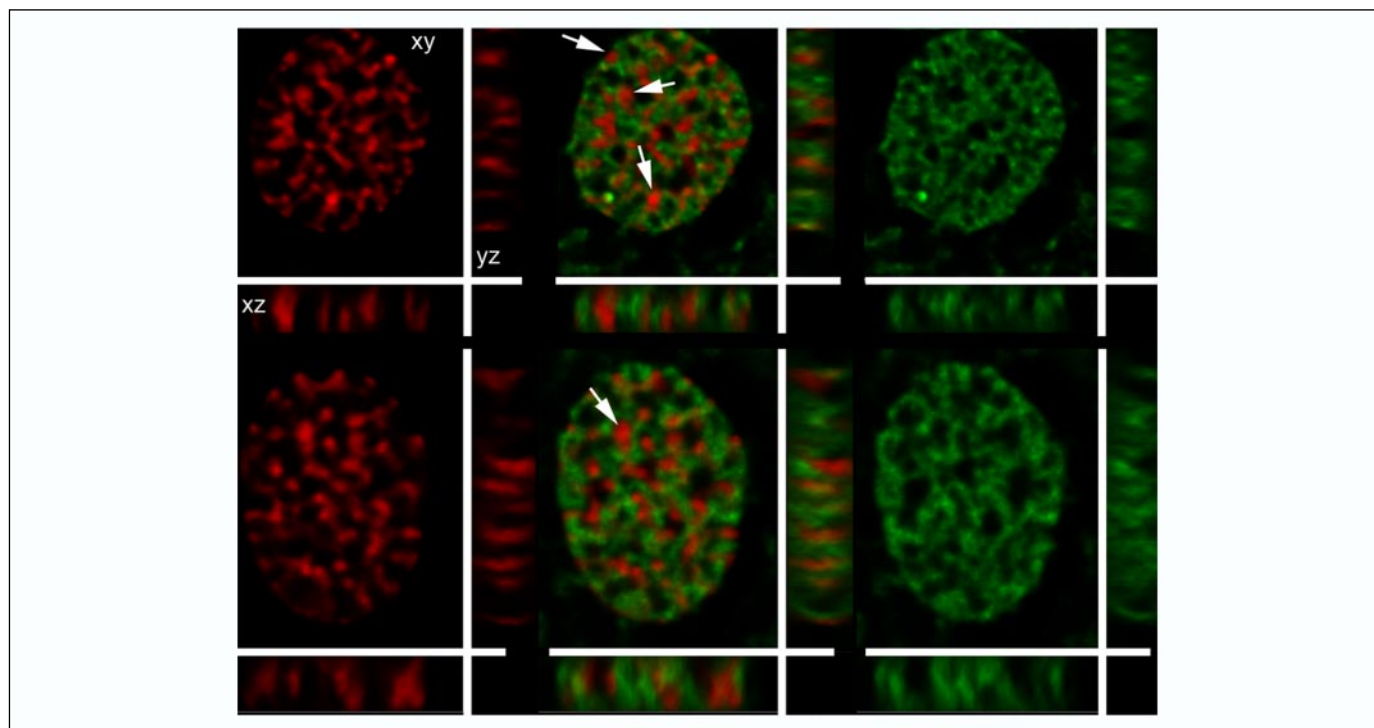


FIGURE 3. **Localization of eGFP-histone H3.3 in postmitotic daughter nuclei.** Mouse 10T1/2 cells stably expressing a histone H3.3-eGFP fusion protein were imaged in culture by indirect immunofluorescence following the addition of Hoechst 33342 to the tissue culture medium. A pair of daughter cells is shown as three-dimensional maximum intensity projections of deconvolved 200-nm z-sections. *xy* (main), *xz* (bottom), and *yz* (right) images are shown in each panel. Each cell is illustrated as a row of images containing the DNA image (red, left panels), the merged channels (middle panels), and the eGFP-histone H3.3 image (right panels). The arrows indicate the positions of pericentromeric heterochromatin.

lish that the phosphorylation status of Ser<sup>10</sup> is not responsible for the observed increase in antibody staining of trimethylated lysine 9.

**Histone H3.3 Does Not Replace H3 Trimethylated at Lysine 9 during Mitotic Exit**—During interphase, tMeK9 has been shown to be displaced from chromatin through the incorporation of histone H3.3 via the replication-independent nucleosome assembly pathway (38). Although this process is likely to be restricted to interphase cells, one recent report demonstrated a small amount of histone H2B exchange during mitosis (39). Thus, it is possible that the incorporation of histone H3.3 occurs specifically during exit from mitosis. To test this hypothesis, we generated 10T1/2 cells stably transfected with eGFP-histone H3.3 and examined their association with pericentromeric heterochromatin during the earliest stages of G<sub>1</sub>, when the interphase nuclei are still decondensing. At this point, the incorporation of histone H3.3 is expected to be maximal if the loss of tMeK9 is dependent upon H3.3 incorporation. Fig. 3 shows deconvolved images of two daughter nuclei in early G<sub>1</sub>. DNA is shown in red, and eGFP-H3.3 is shown in green. Note that at this stage of early G<sub>1</sub>, these cells still partially maintain their metaphase chromosome organization. The arrows indicate regions of pericentromeric heterochromatin, which are easily recognized by their distinctive morphology in mouse fibroblast cell lines. There is no significant incorporation of histone H3.3 into pericentromeric heterochromatin.

**Epitope Accessibility Is Not Responsible for Changes in Trimethylated Lys<sup>9</sup> Abundance during Metaphase**—Perhaps the most obvious explanation for the indirect immunofluorescence results detailed above is the mitotic dissociation of proteins (e.g. heterochromatin protein 1), which may bind to, and mask, a subset of the epitopes during interphase or mitosis. This hypothesis can be easily examined by immunoblotting protein preparations isolated at specific cell cycle stages, where any such proteins will be displaced during SDS-PAGE. To establish that changes in epitope accessibility are not responsible for the methylation dynamics

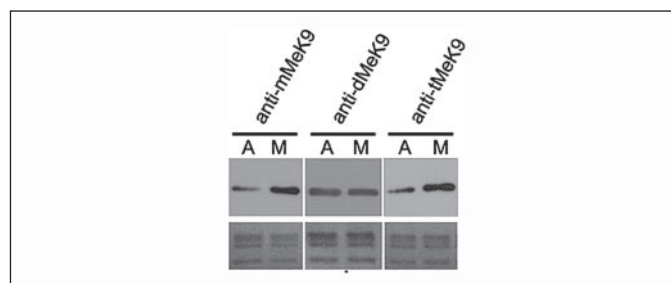
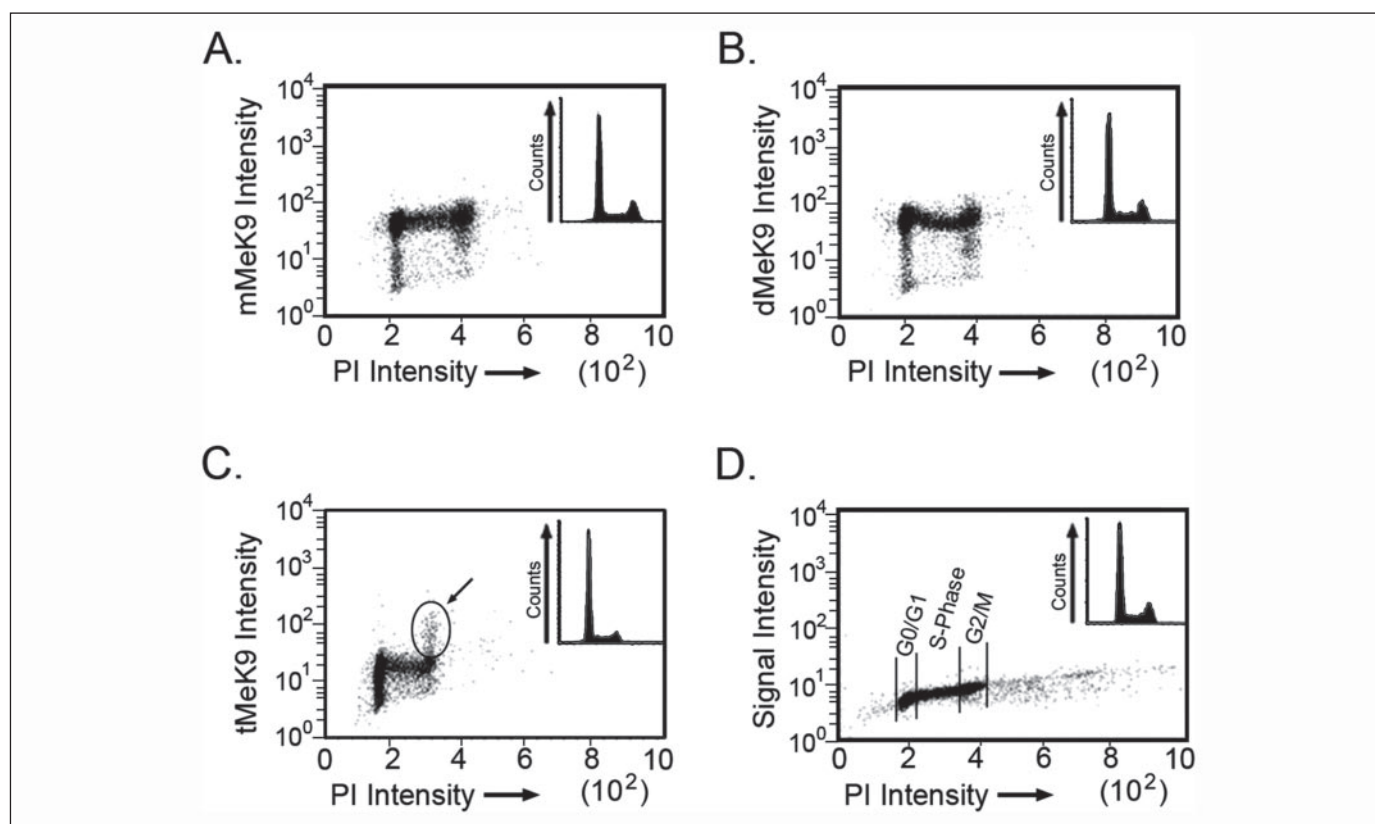


FIGURE 4. **Qualitative assessment of the abundance of various methylated lysine residues at different cell cycle stages.** Immunoblot analysis of nuclear proteins isolated from asynchronously growing (A) or mitotically arrested (M) cells were resolved on 15% SDS-polyacrylamide gels and probed with the antibodies indicated (top). Shown here are representative results from one of three separate experiments. The upper panel (Ab) contains the antibody signal, whereas the lower panel (CPTS) confirms equivalent protein loading by CPTS staining. Qualitative comparisons of methylation signal intensities can only be made within each given antibody treatment.

observed, immunoblotting was performed on acid-extracted proteins isolated from asynchronous or mitotically enriched populations. Approximately  $55.2 \pm 0.8\%$  of asynchronous HeLa cells were in G<sub>0</sub>/G<sub>1</sub>,  $16.9 \pm 0.8\%$  in S-phase, and  $26.7 \pm 1.2\%$  in G<sub>2</sub>/M as determined by flow cytometry. Following overnight treatment with nocodazole, a 3.4-fold increase in the proportion of cells in G<sub>2</sub>/M was observed ( $91.1 \pm 1.6\%$ ), whereas those in G<sub>0</sub>/G<sub>1</sub> ( $3.6 \pm 1.3\%$ ) and S-phase ( $5.4 \pm 0.6\%$ ) were decreased markedly. Microscopy was used to confirm that the cells had accumulated in prometaphase (data not shown). Equivalent protein amounts from the two populations were resolved by SDS-PAGE and immunostained to assess cell cycle-associated differences in the methylated Lys<sup>9</sup> derivatives (Fig. 4). Similar results were obtained with mitotically enriched populations generated by a double thymidine block followed by either nocodazole or ALLN treatment (data not shown). These results confirm that there are significant increases in the abundance of



**FIGURE 5. Cell cycle-dependent progression patterns of methylation epitopes as demonstrated by flow cytometry.** Asynchronous HeLa cells were ethanol-fixed, counterstained with PI to reveal cell cycle status, and independently immunofluorescently labeled with mMeK9 (A), dMeK9 (B), and tMeK9 (C) antibodies. The  $G_0/G_1$ , S-phase and  $G_2/M$  populations are indicated for the PI-only control (D) and can be extrapolated to all other graphs. Shown here is one of three replicates. Each panel plots the fluorescent signal intensity (log scale) of the methylation antibody in arbitrary units against the PI or DNA fluorescence intensity in arbitrary units. The inset in each panel has been included to demonstrate that the cells were actively cycling and provides relative cell counts at each cell cycle stage ( $G_0/G_1$ , S-phase, and  $G_2/M$ ). The arrow in C (tMeK9) identifies the  $G_2/M$  subpopulation with increased signal intensity that is encircled.

mMeK9 and tMeK9 during mitosis. By this approach, the change in the methylation status of dMeK9 appeared to be minimal.

**Global Histone Methylation Dynamics throughout the Cell Cycle**—To better characterize the cell cycle-associated methylation dynamics in asynchronous HeLa cells, we examined each of the three Lys<sup>9</sup> methylation epitopes by flow cytometry (Fig. 5). If Lys<sup>9</sup> methylation is indeed stable, we would expect to observe only a 2-fold increase in total methylation over the course of a cell cycle with the principle methylation intensity decrease coinciding with the 4 to 2 N reduction of the genome during cytokinesis. These relationships are more apparent when expressed as mean intensities for the different stages of the cell cycle ( $G_0/G_1$ , S-phase, and  $G_2/M$ ) after normalizing for DNA content (supplemental Table 1). When expressed this way, the mMeK9 shows a doubling of the labeling intensity when progressing from the 2 N (PI intensity = 200) to 4 N (PI intensity = 400). The dMeK9 remains relatively constant across the cell cycle. In contrast, the tMeK9 isoforms of histone H3 reach peak intensities in  $G_2/M$  (PI intensity = 400) that are greater than expected based on the change in DNA content. Similar results were obtained for 10T1/2 cells (data not shown). Because the  $G_2/M$  peak contains primarily  $G_2$  cells, any change that is confined to cells in prophase through metaphase would not be reflected in the prominent  $G_2/M$  cluster. For example, when histone H3 is phosphorylated at serine 10 or 28, a small number of cells are found to have intensities higher than the main  $G_2/M$  cluster (data not shown). A similar observation can be made in the tMeK9 plot (region circled on the two-dimensional plot) by flow cytometry. Nonetheless, this reflects a limitation of flow cytometry that is overcome when fluorescence microscopy

is used to quantify cell cycle-dependent changes in fluorescence intensity.

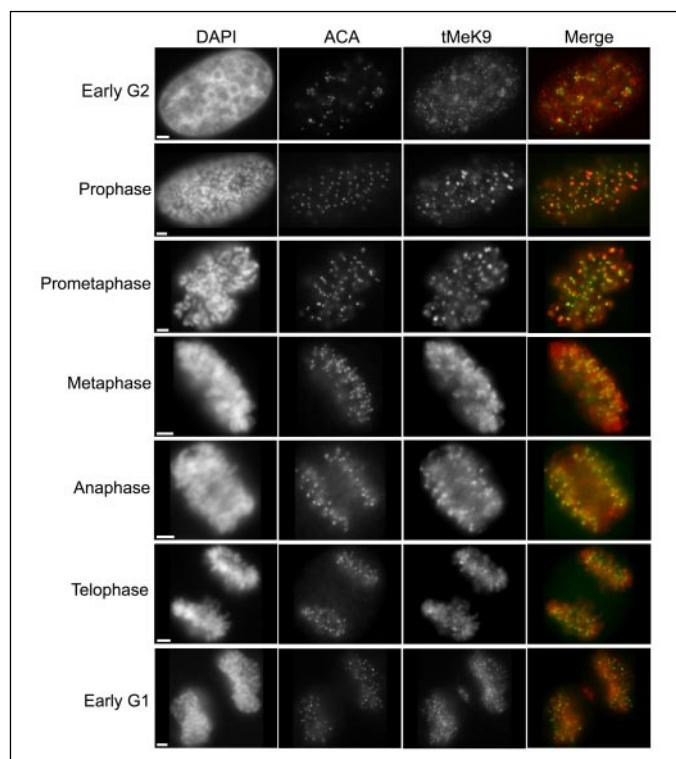
Although the results depicted in Fig. 5 and presented in supplemental Table 1 are consistent with cell cycle-coupled changes in methyl histone content, the variability within any given cell cycle population complicated a direct interpretation of these results. To better understand the cell cycle relationship for each modification, analysis of variance of unweighted means was calculated (Table 1). Similar results were obtained in HeLa cells (data not shown). In all cases, the null hypothesis ( $H_0$ ), that all cell cycle stages exhibit similar mean signal intensities, was rejected. This indicates that at least one cell cycle population mean for each epitope investigated differs significantly from the others. To examine whether these differences were statistically significant, pairwise Tukey-Kramer multicomparison post-tests were performed for each methylation epitope. For all epitopes and between all groups (e.g.  $G_0/G_1$  and S-phase,  $G_0/G_1$  and  $G_2/M$ , and S-phase and  $G_2/M$ ), statistically significant differences ( $p < 0.05$ ) were observed (data not shown). These results validate the previous observations and clearly establish that unique cell cycle dynamics occur for mono-, di-, and trimethylated Lys<sup>9</sup>.

**Quantitative Imaging Microscopy Identifies Mitosis-specific Methylation and Demethylation Cycles in Cycling Cells**—The results above demonstrate that the most striking changes in methylation occur in  $G_2/M$ . To precisely define the temporal progression throughout  $G_2/M$ , quantitative image microscopy was performed (35, 40). In this approach, we were able to resolve, with high temporal resolution, the different stages of mitosis (Fig. 6). The results for mono-, di-, and trimethylated lysine 9 are shown in Fig. 7.

**TABLE 1**

Analysis of variance of unweighted means for methylated histone epitopes in 10T1/2 cells as measured by flow cytometry

Epitope	Group <sup>a</sup>	SS <sup>b</sup>	df <sup>c</sup>	MS <sup>d</sup>	F ratio <sup>e</sup>	p value	Reject H <sub>0</sub> <sup>f</sup>
mMeK9	BG	818,700	2	409,400	10,340	<0.0001	Yes
	WG	693,100	17,499	39.61			
dMeK9	BG	124,000	2	62,020	1329	<0.0001	Yes
	WG	793,900	17,008	46.68			
tMeK9	BG	65,760	2	32,880	758.9	<0.0001	Yes
	WG	735,700	16,979	43.33			

<sup>a</sup> Defines whether or not the analysis is between groups (BG) or within the groups (WG).<sup>b</sup> Sum of squares.<sup>c</sup> Degrees of freedom.<sup>d</sup> Mean square.<sup>e</sup> Calculated by  $MS_{BG}/MS_{WG}$ .<sup>f</sup> The null hypothesis (H<sub>0</sub>) is rejected if the p value is <0.05.

**FIGURE 6. Temporal and spatial progression pattern of tMeK9 through mitosis.** Asynchronously growing HeLa cells were paraformaldehyde-fixed, immunofluorescently labeled with anti-methylated lysine 9 and anti-centromeric antigen (ACA), and counterstained with DAPI. Images were collected as z-series, and only a single representative plane is presented. The tMeK9 signal intensity differences are qualitative between all images, since only that channel was collected using identical exposure times. Scale bar, 3  $\mu$ m.

We identified a similar temporal progression pattern for all three Lys<sup>9</sup> methylation epitopes: increased normalized methylation signal intensities correlated with the entry of cells into mitosis. Normalized methylation TSI reached maximum abundance at metaphase and began to decline as cells entered anaphase. The normalized methylation TSI continued to decrease throughout the later stages of mitosis, until basal steady-state levels were attained by late telophase or early G<sub>1</sub>. Within this group, the largest difference in normalized methylation TSI between interphase and metaphase occurred with tMeK9, where a 4.0-fold difference was observed (supplemental Table 2). The smallest difference observed was for dMeK9 at 1.3-fold, whereas the difference for mMeK9 was 1.4-fold. This was not an artifact of the condensation process, since several other histone methylations tested in this assay (e.g. dMeK4 and tMeK4) did not reveal any appreciable increase or decrease in normalized methylation TSI (data not shown). Subsequent analyses of variance (Table 2) and Tukey-Kramer multicomparison post-tests

(supplemental Table 3) statistically validated the relationships characterized above and confirmed that dramatic changes in the abundance of tMeK9 accompany the entry and the exit of cells from mitosis.

**Dynamic Methylation of Lysine Residues in Developing Mouse Embryos and Primary Tissue Cultures**—To extend our tissue culture observations to an *in vivo* model system, the Lys<sup>9</sup> methylation status of cells from midgestation mouse embryos (embryonic day 9.5) and non-immortalized primary tissue cultures was examined. In both cases, cell cycle-dependent changes in methyl modifications paralleled tissue culture results (data not shown) and also revealed unique developmental correlations for several of the epitopes (see Ref. 41). Perhaps the most striking observation was that the cell cycle-dependent changes observed for tMeK9 in the tissue cultures were more dramatic within the mouse embryo tissue sections. As detailed above, robust tMeK9 staining occurred between prophase and metaphase (Fig. 8). Upon entry into anaphase, the abundance of tMeK9 began to decline until basal levels were reached in interphase. Upon quantification, ratios of Norm-tMeK9 signal intensities between metaphase (0.1464) and either early G<sub>1</sub> (0.02502) or interphase (0.02044) were 5.85 and 7.16, respectively, which represents an ~15-fold increase in total tMeK9 when considered independent of DNA normalization. These results demonstrate that the dynamic changes in tMeK9 observed in mitosis are not specific to tissue culture cells and that the differences appear to be exacerbated *in vivo* in midgestation embryos.

**Cells Lacking tMeK9 Exhibit a Wide Range of Abnormal Mitotic Phenotypes**—Previous investigations by Peters *et al.* (32) demonstrated that deletion of the histone methyltransferases responsible for tMeK9 in mice, namely Suv39h1 and Suv39h2, resulted in an increase in ploidy (e.g. 4 and 8 N). However, the underlying defect manifesting in increased genomic instability was not examined in the Suv39h1/2 dn primary mouse embryonic fibroblasts (MEFs). Nevertheless, Peters *et al.* (32) did observe a failure of the centromeres to segregate properly during mitosis *in vivo* and frequently observed a so-called “butterfly” chromosome morphology. To further address the functional role of tMeK9 in chromosome congression to, and chromosome segregation from, the metaphase plate, we examined mitoses in cells lacking tMeK9 within pericentromeric heterochromatin. We examined mitotic events in control (W8) and Suv39h1/2 dn (D5) IMEFs. Cells lacking Suv39h1/2 have previously been shown to be devoid of tMeK9 staining in pericentromeric heterochromatin (32). We confirmed this phenotype with our anti-tMeK9 antibody (Fig. 9). We examined these cells for aberrant phenotypes associated with metaphase, anaphase, telophase, and cytokinesis/early. Aberrant mitotic phenotypes attributed to the lack of pericentromeric tMeK9 were observed at all mitotic stages and included an increase in misaligned chromosomes in metaphase, nondisjunction in anaphase, lagging chromosomes in telophase, and the appearance of micronuclei at cytokinesis or early G<sub>1</sub> (Fig. 10). Next, we manually



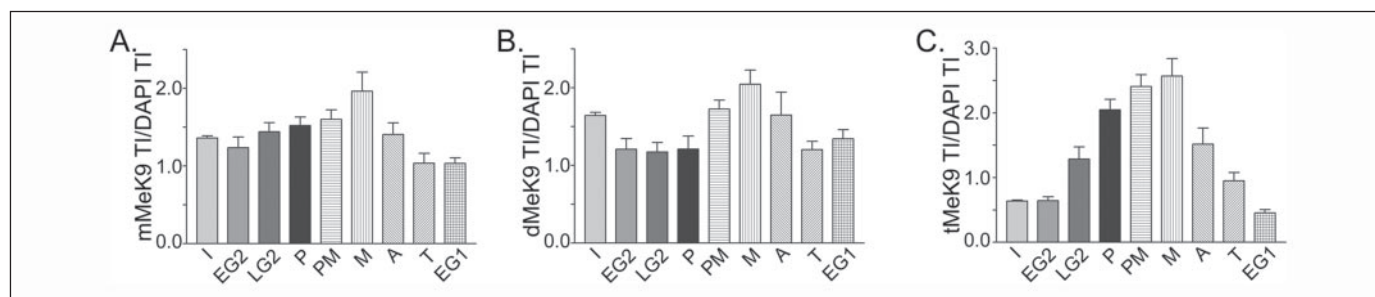


FIGURE 7. **Quantitative comparisons of normalized methylation signal intensities at specific cell cycle stages.** Quantitative image microscopy was performed on 10T1/2 cells immunofluorescently labeled with each methylation antibody: mMeK9 (A), dMeK9 (B), and tMeK9 (C). For each antibody, cells were first classified as belonging to one of nine distinct cell cycle stages: interphase (I), early G<sub>2</sub> (EG2), late G<sub>2</sub> (LG2), prophase (P), prometaphase (PM), metaphase (M), anaphase (A), telophase (T), and early G<sub>1</sub> (EG1). Depicted here are the mean normalized methylation signal intensities (represented as the mean methylation total intensity/mean DAPI total intensity) at each specific cell cycle stage  $\pm$  S.E.

**TABLE 2**

**Analysis of variance tests for the normalized methylation intensities as measured by quantitative imaging microscopy**

Epitope	Group <sup>a</sup>	SS <sup>b</sup>	df <sup>c</sup>	MS <sup>d</sup>	F ratio <sup>e</sup>	p value	Reject H <sub>0</sub> <sup>f</sup>
mMeK9	BG	10.24	8	1.28	5.263	<0.0001	Yes
	WG	101.6	418	0.243			
dMeK9	BG	14.33	8	1.791	3.746	0.0003	Yes
	WG	192.7	403	0.478			
tMeK9	BG	33.9	8	4.237	86.26	<0.0001	Yes
	WG	27.41	558	0.049			

<sup>a</sup> Defines whether or not the analysis is between groups (BG) or within the groups (WG).

<sup>b</sup> Sum of squares.

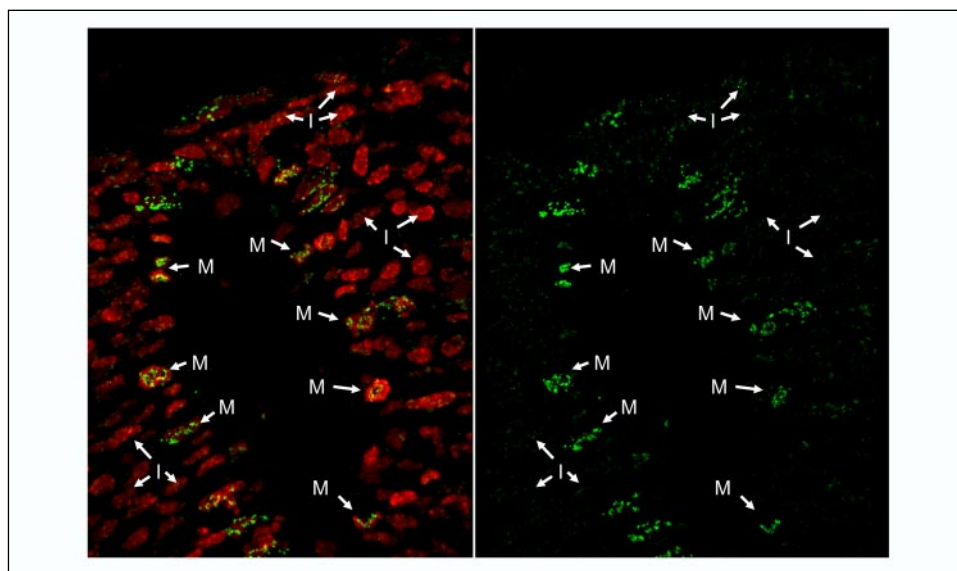
<sup>c</sup> Degrees of freedom.

<sup>d</sup> Mean square.

<sup>e</sup> Calculated by  $MS_{BG}/MS_{WG}$ .

<sup>f</sup> The null hypothesis (H<sub>0</sub>) is rejected if the p value is <0.05.

FIGURE 8. **tMeK9 dynamics during mouse embryonic neural tube development.** A three-dimensional image was collected of the neural tube of an embryonic day 9.4 mouse embryo stained with anti-tMeK9. The three-dimensional image was subjected to deconvolution and is presented as a two-dimensional projection. DNA is counterstained with DAPI (red), and tMeK9 labeling is in green. Shown here is the developing neural tube with the lumen localizing to the central black region devoid of cells. Note the dramatic increase in tMeK9 staining in mitotic cells compared with extremely weak staining in interphase cells. Cells at different stages of the cell cycle, either mitotic (M) or interphase (I), are indicated by the arrows.



scored the normal and aberrant phenotypes in both D5 (Suv39h1/2 dn IMEFs) and W8, and the results are summarized in Table 3. In all cell cycle stages investigated, between 3.3- and 5.2-fold increases in aberrant phenotypes were observed in the D5 cells as compared with the W8 controls (Table 3). The greatest increase in aberrant phenotypes occurred in telophase (5.55-fold increase), where lagging chromosomes were most frequently observed, whereas the smallest increase in aberrant phenotypes was associated with anaphase (3.33-fold increase). Surprisingly however, we did not observe any of the butterfly chromosomes that Peters *et al.* (32) describe for the lymphocytes of the Suv39h-deficient mice; nor did we observe a large increase in ploidy (*i.e.* 4 or 8 N). Rather, we observed significantly greater numbers of misaligned and lagging chromosomes, which would lead to greater levels of aneuploidy.

These findings were further substantiated by comparative flow cytometry performed between D5 and W8 cells labeled with PI, which revealed an overall increase in aneuploidy occurring within the D5 cells (data not shown).

**Protein Methylation Is Required during Entry into Mitosis**—We used an additional approach to confirm the requirement for protein methylation, particularly the generation of tMeK9 during late G<sub>2</sub>, in chromosome segregation. After 2-h treatment with 200  $\mu$ M adenosine dialdehyde, a competitive inhibitor of S-adenosylmethionine that inhibits protein methyltransferases, we observed a 2.5-fold reduction in histone H3 lysine 9 trimethylation in mitotic cells (supplemental Fig. 3A). Some mitotic cells were almost completely devoid of histone lysine 9 trimethylation near centromeres (supplemental Fig. 3C). We also exam-

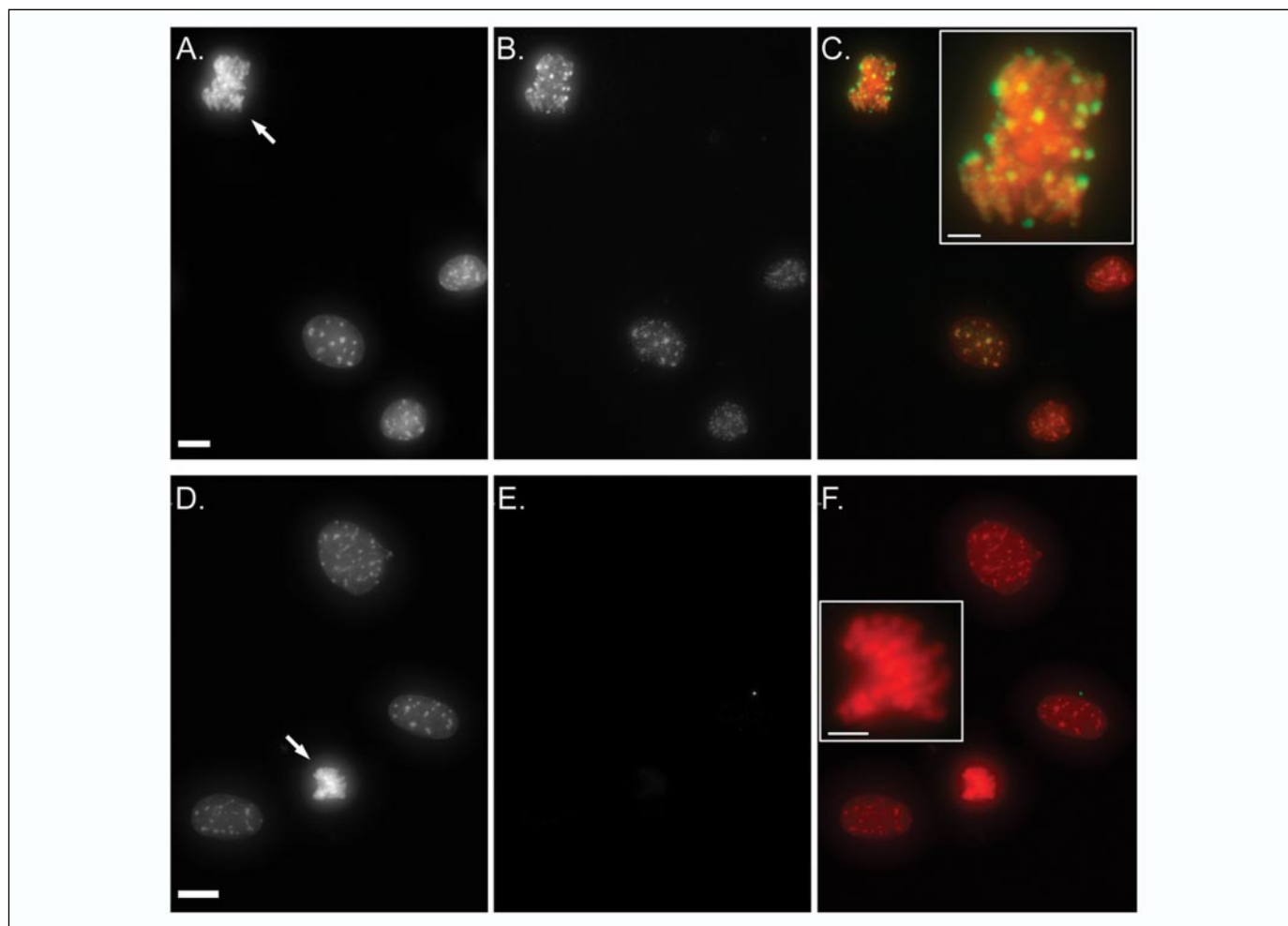


**FIGURE 9. Suv39h1/2 dn IMEFs are devoid of tMeK9 in pericentromeric heterochromatin.** Asynchronous control (W8; A–C) and Suv39h1/2 (D5; D–F) IMEF cells were immunofluorescently labeled with anti-tMeK9 (B and E), and the DNA was counterstained with DAPI (A and D). The merged images are shown in C and F, with red and green representing DAPI and anti-tMeK9, respectively. High resolution images of the mitotic cells are included in the insets of C and F. Identical exposure times were employed in all channels during acquisition and emphasize the dramatic loss of tMeK9 within the pericentromeric heterochromatin of D5 cells (E and F). The arrows indicate the positions of mitotic cells. Scale bars in A and D, 8  $\mu$ m; scale bars in C and F, 2  $\mu$ m.

ined cells for mitotic defects following treatment with a general inhibitor of protein methylation, adenosine dialdehyde. An  $\sim 4$ -fold increase in the number of misaligned and lagging chromosomes was observed following as little as 1 h of incubation with the methyltransferase inhibitor, and this increased to an average of 6.7-fold. This result was obtained from counting over 300 mitotic cells/experiment, following a 2-h incubation with the drug. The defects in chromosome alignment, however, appeared more severe than what was observed in the mouse double null embryonic fibroblast cell lines. Many chromosomes tended to accumulate at the spindle poles (supplemental Fig. 3B, right).

The increased severity of the alignment defects could indicate the presence of compensatory mutations in the embryonic fibroblast cell lines that were necessary to maintain the stability of the cell line. It is equally likely that additional important protein methylations take place specifically during this small window of the cell cycle as cells prepare for entry into mitosis. The trimethylation of histone H4 at lysine 20 is one protein methylation that is a particularly strong candidate. This methylation is also normally enriched in chromatin found near centromeres (see supplemental Fig. 3B, left), and histone H3 lysine 9 trimethylation is required for the efficient targeting of this methylation to the facultative heterochromatin found near centromeres (42). We found that histone H4 lysine 20 trimethylation was also inhibited, although to a lesser

degree than histone H3 lysine 9 trimethylation (supplemental Fig. 3A). Lysine 20 trimethylation is also depleted in the pericentromeric heterochromatin of the double null cell lines (42) (data not shown). Thus, the treatment with the methylation inhibitor does not differ significantly from the knock-out cell line in this respect. Interestingly, the steady-state levels of histone H4 lysine 20 trimethylation were relatively stable during entry into mitosis (supplemental Table 2). The reduction in the abundance of this modification following a 2-h treatment with adenosine dialdehyde indicates that this methylation may nonetheless be quite dynamic throughout this stage of the cell cycle. Thus, there may be other protein methylations, in addition to lysine 9 trimethylation, that are occurring during the  $G_2$  assembly of the centromere and kinetochore complex.

## DISCUSSION

Histone methylation is commonly considered a stable epigenetic mark whose overall pattern and density are transmitted to daughter cells during cell division (15, 18). We examined this hypothesis by exploiting the advantages of quantitative image microscopy to precisely define the relationship between the cell cycle and the relative concentration *in situ* of histone Lys<sup>9</sup> methylations. We documented unexpected dynamics in global methylation as cells progressed through the



## Dynamic Changes in Histone Lysine Methylations

cell cycle in both mammalian tissue culture systems and mouse embryonic tissue sections. Specifically, there was a global increase in mMeK9, dMeK9, and tMeK9 all during the initial stages (late G<sub>2</sub> to prometaphase) of mitosis that reached their maximal densities as chromosomes congressed to the metaphase plate. Although reported to be unchanged during mitosis, Fischle *et al.* (43) showed by quantitative mass spectrometry methods that lysine 9 trimethylation was increased about 2-fold in nocadazole-arrested cells *versus* unsynchronized populations. This increase occurred amid a greater than 100-fold increase in the amount of histone H3 containing both trimethylation at lysine 9 and phosphorylation at serine 10. Our results demonstrate that this methylation is rapidly lost as cells exit mitosis, returning to basal levels by early G<sub>1</sub>. Furthermore, by extending our mammalian tissue culture results to mouse embryonic tissue sections, we find that these cell cycle-dependent changes also occur *in vivo*.

To date, there have been very few studies examining the cell cycle regulation of histone methylation levels. Histone H4 lysine 20 methylation is reported to increase as cells enter mitosis, and this is dependent upon the activity of the PR-Set 7 (44–46). Apart from lysine 20 methylation, most of our current understanding of methylation dynamics

was obtained during the late 1960s and early 1970s using radioactive tracers in methyl donors, including *S*-adenosyl-L-methionine and methionine. The labeled methyl donors were added to living cells and incorporated into histone N termini at lysine residues, and label turnover was investigated. By following the amount of radiolabel incorporated into each histone and determining the rate at which it was lost, the turnover of the radiolabeled modifications was calculated. Although the analysis of histone methylation was limited to the study of the individual histone subtypes (e.g. H3 or H4) and not the specific residue or level (e.g. mono-, di-, or trimethylation), these studies did reveal evidence for methylation turnover as well as a potential peak in histone methyltransferase activity that corresponds with G<sub>2</sub>- and M-phase (47, 48). An enzyme, LSD1, was recently reported to be responsible for the removal of dimethylation (29, 31). Although this enzyme cannot remove trimethylation from lysine, a second family of proteins, protein hydroxylases, may be capable of removing trimethylation from lysines (49).

Genetic modulation of Suv39h1 expression levels directly impacts the abundance of tMeK9 localizing within the pericentromeric heterochromatin and adversely affects the fidelity of mitosis. For example, Suv39h1 overexpression, accompanied by experimentally induced increases in tMeK9, is associated with defects in mitotic progression and chromosome segregation (50). Conversely, mice lacking Suv39h1/2, which do not exhibit tMeK9 within pericentromeric heterochromatin, exhibit increased genomic instabilities and cancer predispositions that presumably arise by increases in ploidy (e.g. 4 or 8 N) (32, 51). Although mitotic spreads of cells isolated from spontaneously arising lymphomas in Suv39h1/2-deficient mice were found to contain an abundance of butterfly chromosomes (32, 52), neither the underlying mechanism(s) responsible for the mitotic defect nor the specific function(s) of this mitotic methylation have been characterized previously. When we analyzed the mitotic progression in Suv39h1/2 dn IMEFs, the absence of pericentromeric tMeK9 correlated with an increase in abnormal mitoses. However, these aberrant phenotypes were distinct from those described by Peters *et al.* (32, 52). For instance, we observe chromosome misalignment, nondisjunction, and lagging chromosomes more frequently in Suv39h1/2 dn IMEFs (D5) than in control IMEFs (W8) as well as in HeLa cells treated for 2 h with the protein methyltransferase inhibitor, adenosine dialdehyde. The simplest interpretation of our results is that tMeK9 dynamics are essential for some aspect of centromere/kinetochore structure or function or essential for the maintenance of chromosome cohesion during initial mitotic stages. Our results are consistent with the established requirement for tMeK9 in the recruitment of cohesin subunits to centromeric repeats in fission yeast, where abrogation of tMeK9 has been shown to lead to premature sister chromatid separation and chromosome missegregation (53, 54).

The robust loss of histone methylation as cells exit mitosis was particularly unexpected, since this methylation has not been shown previously to turn over. We investigated an alternative mechanism of

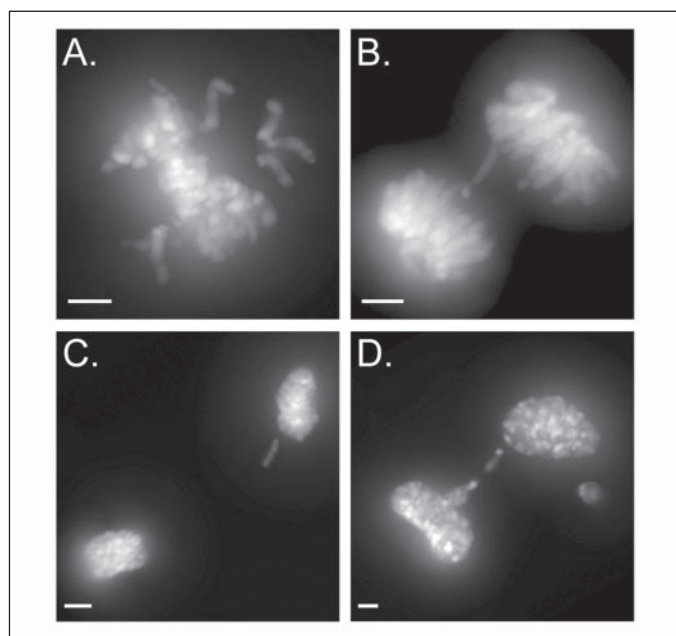


**FIGURE 10. Typical abnormal mitotic phenotypes observed in the absence of trimethylated lysine 9 (H3).** High resolution ( $\times 100$ ) digital image micrographs of representative abnormal mitotic phenotypes associated with the lack of trimethylated lysine 9 (H3) in Suv39h1/2 dn IMEFs. Suv39h1/2 dn IMEFs were fixed and counterstained with DAPI to reveal mitotic abnormalities. Depicted here are two-dimensional projections of misaligned chromosomes during metaphase (A), nondisjunction during anaphase (B), lagging chromosome during telophase (C), and lagging chromosomes and the appearance of micronuclei in cytokinesis or early G<sub>1</sub> (D).

**TABLE 3**  
Mitotic aberrations in Suv39h1/2 dn IMEFs

Stage	Category <sup>a</sup>	IMEF control (W8)		Suv39h1/2 <sup>-/-</sup>		Difference
		Percentage	Number of cells	Percentage	Number of cells	
		%		%		-Fold
Metaphase	N	96.14	523	84.36	151	4.05
	A	3.86	21	15.3	28	
Anaphase	N	95.83	161	85.51	62	3.33
	A	4.17	7	14.49	10	
Telophase	N	96.53	195	76.03	105	5.55
	A	3.47	7	23.97	25	
Cytokinesis/ Early G <sub>1</sub>	N	95.88	489	84.89	389	3.43
	A	4.12	21	15.11	64	

<sup>a</sup> N, normal phenotype; A, aberrant phenotype.

replacement, the possibility that replication-independent nucleosome assembly or histone replacement could potentially account for the decrease in tMeK9 we observe as cells exit mitosis. Outside of S-phase or DNA replication, the unincorporated pool of histone H3 is predominated by the histone H3 sequence variant H3.3 (55, 56). In rapidly growing tissue culture cell lines and short lived but terminally differentiated cells *in vivo*, histone H3.3 is known to accumulate in regions of chromatin that are transcriptionally active (26, 57, 58). In longer lived postreplicative cells, such as neurons, histone H3.3 can become the predominant histone H3 incorporated into chromatin (55). Therefore, replication-independent nucleosome assembly or histone replacement provides the only known mechanism of tMeK9 removal. Recently, Janicki *et al.* (38) demonstrated that H3.3 *in vivo* could replace tMeK9-containing H3 but only upon transcriptional activation. Although the replacement of preexisting chromatinized histone H3 with histone H3.3 is an event thought to be both transcription-dependent and restricted to interphase, we examined the possibility that a previously unknown replacement of chromatinized histone H3 with histone H3.3 within pericentromeric heterochromatin may occur during this brief period of mitosis. As expected, we found no evidence for the presence of histone H3.3 in pericentromeric heterochromatin, consistent with a previous report demonstrating that histone H3.2 is the major histone H3 species present in the pericentromeric heterochromatin of mice (59). Thus, the loss of tMeK9 as cells exit mitosis is most easily explained by a demethylation event that is particularly robust during this very brief period of the cell cycle (~15–30 min). A further characterization of the demethylation and its functional significance must await the identification of the enzyme or enzymes responsible.

**Acknowledgments**—We thank Drs. T. Jenuwein (Institute of Molecular Pathology, Vienna), Gordon K. T. Chan (University of Alberta, Edmonton, Canada), and John Th'ng (Northwestern Ontario Regional Cancer Center) for generously providing the D5/W8 IMEFs, anti-centromeric antigen antibody, and H3.3-eGFP expressing cells, respectively, and Abcam for supplying the methylation antibodies and peptides. We thank Dr. X. Sun and J. Wizniak for helpful discussions and technical assistance.

## REFERENCES

- Zhang, L., Eugeni, E. E., Parthun, M. R., and Freitas, M. A. (2003) *Chromosoma* **112**, 77–86
- Goll, M. G., and Bestor, T. H. (2002) *Genes Dev.* **16**, 1739–1742
- Sims, R. J., III, Nishioka, K., and Reinberg, D. (2003) *Trends Genet.* **19**, 629–639
- Brehm, A., Tufeland, K. R., Aasland, R., and Becker, P. B. (2004) *BioEssays* **26**, 133–140
- Cavalli, G., and Paro, R. (1998) *Curr. Opin. Cell Biol.* **10**, 354–360
- Eissenberg, J. C. (2001) *Gene (Amst.)* **275**, 19–29
- Zeng, L., and Zhou, M. M. (2002) *FEBS Lett.* **513**, 124–128
- Murray, K. (1964) *Biochemistry* **127**, 10–15
- Paik, W. K., and Kim, S. (1967) *Biochem. Biophys. Res. Commun.* **29**, 14–20
- Lachner, M., and Jenuwein, T. (2002) *Curr. Opin. Cell Biol.* **14**, 286–298
- Bannister, A. J., Schneider, R., and Kouzarides, T. (2002) *Cell* **109**, 801–806
- van Leeuwen, F., Gafken, P. R., and Gottschling, D. E. (2002) *Cell* **109**, 745–756
- Ng, H. H., Feng, Q., Wang, H., Erdjument-Bromage, H., Tempst, P., Zhang, Y., and Struhl, K. (2002) *Genes Dev.* **16**, 1518–1527
- Rice, J. C., and Allis, C. D. (2001) *Curr. Opin. Cell Biol.* **13**, 263–273
- Bannister, A. J., Zegerman, P., Partridge, J. F., Miska, E. A., Thomas, J. O., Allshire, R. C., and Kouzarides, T. (2001) *Nature* **410**, 120–124
- Fischle, W., Wang, Y., Jacobs, S. A., Kim, Y., Allis, C. D., and Khorasanizadeh, S. (2003) *Genes Dev.* **17**, 1870–1881
- Jacobs, S. A., Taverna, S. D., Zhang, Y., Briggs, S. D., Li, J., Eissenberg, J. C., Allis, C. D., and Khorasanizadeh, S. (2001) *EMBO J.* **20**, 5232–5241
- Lachner, M., O'Carroll, D., Rea, S., Mechtler, K., and Jenuwein, T. (2001) *Nature* **410**, 116–120
- Nakayama, J., Rice, J. C., Strahl, B. D., Allis, C. D., and Grewal, S. I. (2001) *Science* **292**, 110–113
- Kiekhäfer, C. M., Grass, J. A., Johnson, K. D., Boyer, M. E., and Bresnick, E. H. (2002) *Proc. Natl. Acad. Sci. U. S. A.* **99**, 14309–14314
- Litt, M. D., Simpson, M., Gaszner, M., Allis, C. D., and Felsenfeld, G. (2001) *Science* **293**, 2453–2455
- Noma, K., Allis, C. D., and Grewal, S. I. (2001) *Science* **293**, 1150–1155
- Santos-Rosa, H., Schneider, R., Bannister, A. J., Sherriff, J., Bernstein, B. E., Emre, N. C., Schreiber, S. L., Mellor, J., and Kouzarides, T. (2002) *Nature* **419**, 407–411
- Byvoet, P., Shepherd, G. R., Hardin, J. M., and Noland, B. J. (1972) *Arch. Biochem. Biophys.* **148**, 558–567
- Duerre, J. A., and Lee, C. T. (1974) *J. Neurochem.* **23**, 541–547
- Waterborg, J. H. (1993) *J. Biol. Chem.* **268**, 4918–4921
- Cuthbert, G. L., Daujat, S., Snowden, A. W., Erdjument-Bromage, H., Hagiwara, T., Yamada, M., Schneider, R., Gregory, P. D., Tempst, P., Bannister, A. J., and Kouzarides, T. (2004) *Cell* **118**, 545–553
- Wang, Y., Wysocka, J., Sayegh, J., Lee, Y. H., Perlin, J. R., Leonelli, L., Sonbuchner, L. S., McDonald, C. H., Cook, R. G., Dou, Y., Roeder, R. G., Clarke, S., Stallcup, M. R., Allis, C. D., and Coonrod, S. A. (2004) *Science* **306**, 279–283
- Shi, Y., Lan, F., Matson, C., Mulligan, P., Whetstone, J. R., Cole, P. A., and Casero, R. A. (2004) *Cell* **119**, 941–953
- Bannister, A. J., and Kouzarides, T. (2005) *Nature* **436**, 1103–1106
- Metzger, E., Wissmann, M., Yin, N., Muller, J. M., Schneider, R., Peters, A. H., Gunther, T., Buettner, R., and Schule, R. (2005) *Nature* **437**, 436–439
- Peters, A. H., O'Carroll, D., Scherthan, H., Mechtler, K., Sauer, S., Schofer, C., Weipoltshammer, K., Pagani, M., Lachner, M., Kohlmaier, A., Opravil, S., Doyle, M., Sibilia, M., and Jenuwein, T. (2001) *Cell* **107**, 323–337
- Aagaard, L., Schmid, M., Warburton, P., and Jenuwein, T. (2000) *J. Cell Sci.* **113**, 817–829
- Todaro, G. J., and Green, H. (1963) *J. Cell Biol.* **17**, 299–313
- McManus, K. J., and Hendzel, M. J. (2003) *Mol. Cell Biol.* **23**, 7611–7627
- Bickar, D., and Reid, P. D. (1992) *Anal. Biochem.* **203**, 109–115
- Hendzel, M. J., Wei, Y., Mancini, M. A., Van Hooser, A., Ranalli, T., Brinkley, B. R., Bazett-Jones, D. P., and Allis, C. D. (1997) *Chromosoma* **106**, 348–360
- Janicki, S. M., Tsukamoto, T., Salghetti, S. E., Tansey, W. P., Sachidanandam, R., Prasanth, K. V., Ried, T., Shav-Tal, Y., Bertrand, E., Singer, R. H., and Spector, D. L. (2004) *Cell* **116**, 683–698
- Thiriet, C., and Hayes, J. J. (2005) *Genes Dev.* **19**, 677–682
- McManus, K. J., and Hendzel, M. J. (2005) *Methods* **36**, 351–361
- Biron, V. L., McManus, K. J., Hu, N., Hendzel, M. J., and Underhill, D. A. (2004) *Dev. Biol.* **276**, 337–351
- Schotta, G., Ebert, A., Krauss, V., Fischer, A., Hoffmann, J., Rea, S., Jenuwein, T., Dorn, R., and Reuter, G. (2002) *EMBO J.* **21**, 1121–1131
- Fischle, W., Tseng, B. S., Dormann, H. L., Ueberheide, B. M., Garcia, B. A., Shabanowitz, J., Hunt, D. F., Funabiki, H., and Allis, C. D. (2005) *Nature* **438**, 1116–1122
- Julien, E., and Herr, W. (2004) *Mol. Cell* **14**, 713–725
- Karachentsev, D., Sarma, K., Reinberg, D., and Steward, R. (2005) *Genes Dev.* **19**, 431–435
- Rice, J. C., Nishioka, K., Sarma, K., Steward, R., Reinberg, D., and Allis, C. D. (2002) *Genes Dev.* **16**, 2225–2230
- Annunziato, A. T., Eason, M. B., and Perry, C. A. (1995) *Biochemistry* **34**, 2916–2924
- Borun, T. W., Pearson, D., and Paik, W. K. (1972) *J. Biol. Chem.* **247**, 4288–4298
- Treweek, S. C., McLaughlin, P. J., and Allshire, R. C. (2005) *EMBO Rep.* **6**, 315–320
- Melcher, M., Schmid, M., Aagaard, L., Selenko, P., Laible, G., and Jenuwein, T. (2000) *Mol. Cell Biol.* **20**, 3728–3741
- Cheutin, T., McNairn, A. J., Jenuwein, T., Gilbert, D. M., Singh, P. B., and Misteli, T. (2003) *Science* **299**, 721–725
- Gonzalo, S., Garcia-Cao, M., Fraga, M. F., Schotta, G., Peters, A. H., Cotter, S. E., Eguia, R., Dean, D. C., Esteller, M., Jenuwein, T., and Blasco, M. A. (2005) *Nat. Cell Biol.* **7**, 420–428
- Partridge, J. F., Scott, K. S., Bannister, A. J., Kouzarides, T., and Allshire, R. C. (2002) *Curr. Biol.* **12**, 1652–1660
- Volpe, T., Schramke, V., Hamilton, G. L., White, S. A., Teng, G., Martienssen, R. A., and Allshire, R. C. (2003) *Chromosome Res.* **11**, 137–146
- Bosch, A., and Suau, P. (1995) *Eur. J. Cell Biol.* **68**, 220–225
- Hendzel, M. J., and Davie, J. R. (1990) *Biochem. J.* **271**, 67–73
- Ahmad, K., and Henikoff, S. (2002) *Mol. Cell* **9**, 1191–1200
- Jackson, V. (1990) *Biochemistry* **29**, 719–731
- Russanova, V., Stephanova, E., Pashev, I., and Tsanev, R. (1989) *Mol. Cell Biochem.* **90**, 1–7

**Dynamic Changes in Histone H3 Lysine 9 Methylations: IDENTIFICATION OF A MITOSIS-SPECIFIC FUNCTION FOR DYNAMIC METHYLATION IN CHROMOSOME CONGRESSION AND SEGREGATION**

Kirk J. McManus, Vincent L. Biron, Ryan Heit, D. Alan Underhill and Michael J. Hendzel

*J. Biol. Chem.* 2006, 281:8888-8897.

doi: 10.1074/jbc.M505323200 originally published online December 21, 2005

---

Access the most updated version of this article at doi: [10.1074/jbc.M505323200](https://doi.org/10.1074/jbc.M505323200)

Alerts:

- [When this article is cited](#)
- [When a correction for this article is posted](#)

[Click here](#) to choose from all of JBC's e-mail alerts

Supplemental material:

<http://www.jbc.org/content/suppl/2005/12/23/M505323200.DC1>

This article cites 59 references, 21 of which can be accessed free at

<http://www.jbc.org/content/281/13/8888.full.html#ref-list-1>